CrystEngComm

Accepted Manuscript

This is an *Accepted Manuscript*, which has been through the Royal Society of Chemistry peer review process and has been accepted for publication.

Accepted Manuscripts are published online shortly after acceptance, before technical editing, formatting and proof reading. Using this free service, authors can make their results available to the community, in citable form, before we publish the edited article. We will replace this *Accepted Manuscript* with the edited and formatted *Advance Article* as soon as it is available.

You can find more information about *Accepted Manuscripts* in the Information for Authors.

Please note that technical editing may introduce minor changes to the text and/or graphics, which may alter content. The journal's standard Terms & Conditions and the Ethical guidelines still apply. In no event shall the Royal Society of Chemistry be held responsible for any errors or omissions in this *Accepted Manuscript* or any consequences arising from the use of any information it contains.

ROYAL SOCIETY OF CHEMISTRY

www.rsc.org/crystengcomm

CrystEngComm RSCPublishing

ARTICLE

Low-Temperature Crystal Growth of Aluminium-Doped Zinc Oxide Nanoparticles in a Melted Viscous Liquid of Alkylammonium Nitrates for Fabrication of Their Transparent Crystal Films†

Cite this: DOI: 10.1039/x0xx00000x

Hiroki Kaneko,[a] Takanari Togashi,[a] Takashi Naka,[b] Manabu Ishizaki,[a] Katsuhiko Kanaizuka,[a] Masatomi Sakamoto[a] and Masato Kurihara*[a]

DOI: 10.1039/x0xx00000x

www.rsc.org/

We fabricated conductive Al-doped ZnO (AZO) films on glass substrates *via* a simple drop-coating process of alcoholic dispersion solutions of AZO nanoparticles of less than 10 nm in dimension, which were prepared by hydrolysis reactions of $Zn(NO_3)_2 \cdot 6H_2O$ and $Al(NO_3)_3 \cdot 9H_2O$ with an excess amount of isopropylamine. After a process of heating at 150ºC to completely remove the alcoholic solvent, a by-product, isopropylammonium nitrate, still remained, was melted, and functioned as a low-temperature medium for the AZO nanoparticles. Even in the low-temperature medium at 150ºC, the AZO nanoparticles could readily grow up ~100 nm, based on Ostwald ripening as a plausible crystal growth mechanism. The medium could be evaporated at 240ºC, and a highly transparent AZO film appeared on the glass with a transmittance of ~83% in the visible region. The electric conductivity of the AZO films was improved by sintering at 450ºC and post-annealing at 450°C in a stream of a mixed gas of N_2 and H_2. The resistivity of the AZO film reached 4.3×10^{-2} Ω cm in a suitable case of Al/Zn molar ratio of 2.0%.

1 Introduction

Metal oxides have been versatile and indispensable materials for industrial applications using catalytic,[1,2] electrical,[3-7] optical,[8-10] magnetic, [11] and their hybrid natures. In order to adopt the metal oxides as functional components for various electronic devices, controlling the thickness and nanometre-scaled fine structures of their films has become an important technology.[12,13] High-performance metal oxide films have been successfully prepared by dry processes such as sputtering,[14,15] pulsed laser deposition,[16,17] and chemical vapour deposition.[18] The crystal growth and metal compositions of the metal oxide films have been controlled on a variety of substrates with atomic-level purities; nevertheless, these dry processes would be categorised as an energy-consuming technique.

The current trend towards green chemistry has prompted our chemists to develop precursor solutions of the functional components for electronic devices. In particular, the advent of printed electronics has necessitated precursor solutions suitable for low-temperature solution processes using printing technologies.[19] Dispersion solutions of nanoparticles are some of the most promising precursor solutions. In a typical case, silver nanoparticles can be readily coated on substrates using their dense dispersion solutions and undergo crystal growth *via* fusing into each other by low-temperature heating processes at 150ºC or less.[19,20] Low-temperature crystal growth is realised on conductive metal circuits of heat-sensitive commodity plastics, such as polyethylene terephthalate (PET), moving towards the next-generation flexible electronic devices.[19,20]

Film formations, along with the low-temperature crystal growth of metal oxides, have been achieved by repeated spray-, spin-, or drop-coating using precursor solutions followed by pyrolysis reactions of the precursor metal complexes and/or metal salts.[21] These repeated coating and heating processes are generally time-consuming methods for fabricating thick films of metal oxides. Dense dispersion solutions and/or pastes of metal oxide nanoparticles will be good candidates for the preparation of their thick films on substrates;[22,23] however, low-temperature crystal growth of the metal oxides is difficult, even after successful removal of the dispersion media and the surface-protecting molecules, due to the intrinsically large lattice energy of the metal oxides as ionic crystals. If the

CrystEngComm Accepted Manuscript

surface-protecting organic molecules are incompletely removed from the metal oxide nanoparticles, thermal decomposition of the remaining organic molecules partially blackens the metal oxide films by the carbon components.[22]

The metal oxide nanoparticles are allowed to be larger in size *via* the Ostwald ripening growth mechanism at a relatively low temperature under pressurised hydrothermal and aqueous solution conditions with controlled pH.[23-26] In the crystal growth processes of the metal oxide nanoparticles, the coordination bond energy of water and/or the additive ligands contributes to the etching of the surface metal ions from the nanoparticles against the large lattice energy.[27] As a possible low-temperature solution process, the metal oxide films have been formed through crystal growth on the substrates, where the substrates are immersed over a long time period in aqueous solutions containing metal salts with additive ligands at a controlled pH condition.[27]

In this study, we have proposed a low-temperature method for the crystal growth of Al-doped zinc oxide (AZO) nanoparticles[25,28-33] on glass substrates *via* a simple process of drop coating their alcoholic dispersion solutions. After removing the alcoholic medium, the AZO nanoparticles were still dispersed in a viscous liquid of isopropylammonium nitrates ($(C_3H_7NH_3)NO_3$) melting at 150ºC. The liquid of the $(C_3H_7NH_3)NO_3$ was homogeneously spread on the glass substrate, and it functioned as a potential medium for low-temperature crystal growth of the AZO nanoparticles at 150ºC. The crystal growth mechanism of the AZO nanoparticles has been discussed based on Ostwald ripening. The $(C_3H_7NH_3)NO_3$ salts could be completely evaporated at elevated temperatures up to 240ºC to provide AZO films consisting of submicrometre-sized crystals. The thickness of the AZO films could be conveniently controlled, depending on the volumes of the drop-coated alcoholic dispersion solutions.

2 Experimental

2.1 Materials

Guaranteed grades of $Zn(NO_3)_2{\cdot}6H_2O$, $Al(NO_3)_3{\cdot}9H_2O$, isopropylamine, ethanol, and *n*-butanol were purchased from Kanto Chemicals. Extra pure grade methanol was obtained from Kanto Chemicals. All reagents were used as supplied without purification.

2.2 Preparation of precursor dispersion solutions of AZO nanoparticles

$Zn(NO_3)_2{\cdot}6H_2O$ (1.50 g, 5.05 mmol) was dissolved into a mixed solvent of methanol and ethanol (12 mL, 1:1 v/v). For the purpose of doping Al^{3+}, appropriate amounts of $Al(NO_3)_3{\cdot}9H_2O$ from 1.0 to 5.0 mol% on the basis of Zn^{2+} were added to the zinc nitrate solutions. After the addition of isopropylamine (0.895 g, 15.2 mmol) to the solutions, they were changed into white suspensions, where isopropylamines acted as an alkali agent to generate AZO nanoparticles and their surface-protecting molecules. The suspensions were further stirred at 60ºC for 10 min to complete the hydrolysis reaction for forming AZO nanoparticles and $(C_3H_7NH_3)NO_3$. The white suspensions were diluted with *n*-butanol (6.0 mL) and were stirred at 60ºC for 60 min to improve the dispersibility of the AZO nanoparticles. Their dispersibility was maintained between several hours and one day, depending on the doping molar ratios of Al. The as-prepared white cloudy dispersion solutions that contained the AZO nanoparticles were immediately employed as precursor solutions of AZO sintering films on glass substrates.

2.3 Isolation and characterisation of AZO nanoparticles

In a typical case, 2 mol% Al-doped zinc oxide (2% AZO) nanoparticles dispersed in the precursor solution were centrifuged at 1570 G for 10 min (a Kubota 3780 centrifuge separator). The isolated nanoparticles were suspended again in methanol, collected *via* a similar centrifugation procedure for purification, and dried under reduced pressure. The as-obtained white solids of the AZO nanoparticles were subjected to powder X-ray diffraction (XRD) analysis using a Rigaku SmartLab X-ray diffractometre and thermogravimetric (TG) analysis using a TA Instruments SDT Q600 under a stream of He. The liberated gasses from the white solids synchronised with the TG weight loss were directly transferred into a JEOL JEM-Q1050 mass spectrometre to investigate the surface-protecting molecules of the AZO nanoparticles. Fourier transform infrared (FT-IR) spectra of the white solids were obtained from a Thermo Scientific Nicolet 6700 FT-IR spectrometre. AZO nanoparticles were observed on a JEOL JEM-2100F field emission transmission electron microscope (FE-TEM), where a diluted methanol suspension was dropped on a carbon-coated copper grid to obtain the FE-TEM sample. The elemental distribution (EDS mapping) of the AZO nanoparticles was also investigated using an energy dispersive X-ray (EDX) analyser (JEOL JED-2300) for scanning transmission microscope images (STEM-HAADF images) through a high-angle annular dark-field (HAADF) detector. The doping molar ratio of Al was estimated by X-ray fluorescence (XRF) analysis using a Rigaku Primini wavelength dispersive X-ray (WDX) spectrometre.

2.4 Preparation of AZO sintering films using precursor dispersion solutions

The precursor dispersion solution (400 μL) containing AZO nanoparticles heated at 60ºC was dropped on a glass substrate (28 × 48 mm) treated under ultrasonification in soapy water, deionised water, and methanol, and then dried in a flow of air. The drop-coated substrate was heated at 150ºC for 10 min on a hot plate to evaporate the solvent of the precursor solution. The transparent liquid matter, melted $(C_3H_7NH_3)NO_3$, remained on the glass substrate, which functioned as a medium for AZO nanoparticles. At an elevated temperature of 240ºC, the $(C_3H_7NH_3)NO_3$ medium was removed within 10 min *via* decomposition and/or vaporisation. The resulting AZO solid film was sintered at 450ºC for 60 min. To control the thickness of the AZO films, various volumes from 100 to 1000 μL of the precursor solutions were dropped on glass substrates.

CrystEngComm Accepted Manuscript

 This journal is © The Royal Society of Chemistry 2012

2.5 Improvement of electrical conductivity of AZO sintering films by post-annealing with H_2

AZO sintering films using the precursor solutions were post-annealed at 450ºC for 90 min using an Ulvac MILA-5000 infrared furnace in a stream (1.0 L/min) of a mixed gas of N_2 and H_2 (N_2/H_2 = 96 : 4 v/v), where water was electrolysed to generate the H_2 gas by using a YMC YH-500 hydrogen gas generator.

2.6 Characterisation of AZO sintering films

The sheet resistance of the sintering films was measured *via* the four-point probe technique using a Kyowariken K-705RS resistivity metre. The transmittance of the sintering films was recorded on a Shimadzu UV-3150 UV/VIS/NIR spectrometre. The anisotropic nature and single crystalline sizes of the AZO on the glass substrate were investigated by XRD analyses. The surface and cross-section morphologies were obtained as field emission scanning electron microscope (FE-SEM) images from a JEOL JSM-7600F. The electron density, mobility, and volume resistance of the AZO sintering films were measured using a Quantum Design physical properties measurement system, which can generate magnetic fields within (plus minus) 5 tesla.

3 Results and Discussion

3.1 Preparation of precursor dispersion solutions of AZO nanoparticles and their characterisations

$Zn(NO_3)_2$ and $Al(NO_3)_3$ dissolved in the alcoholic solvent of methanol and ethanol underwent hydrolysis reaction through their crystal and/or coordination water molecules by the addition of excess amounts of isopropylamine as seen in the following equations (1) and (2):

$$Zn(NO_3)_2+H_2O+2C_3H_7NH_2 \rightarrow ZnO+2(C_3H_7NH_3)NO_3 \quad (1)$$

$$2Al(NO_3)_3+3H_2O+6C_3H_7NH_2 \rightarrow Al_2O_3+6(C_3H_7NH_3)NO_3 \quad (2)$$

The suspended white particles of AZO were immediately precipitated. The poor dispersibility of the particles could be improved by adding *n*-butanol for dilution and stirring at 60ºC for 60 min as a post treatment. Dispersibility was maintained for up to one day without any precipitation; nevertheless, there was a tendency towards lesser dispersibility as the doping molar ratios of Al increased. Fig. 1 shows TEM images and a selected area electron diffraction (SAED) image of the white particles centrifugally isolated from the precursor solution containing a 2% doping molar ratio of Al. Six rings observed from the SAED image (Fig. 1a) match with the hexagonal ZnO crystals.[30] Based on a lower magnification TEM image, the average size of the isolated white particles was estimated to be 5.8 ± 0.6 nm (Fig. 1b and 1c). Lattice fringes were clearly observed in the nanoparticles from a higher magnification TEM image (Fig. 1d), and they had a high crystallinity without any grain boundaries as single crystals. The fringe patterns can be indexed to d_{100} = 0.291, d_{002} = 0.261, and d_{101} = 0.253 nm. The high-quality and -crystallinity colloidal AZO nanoparticles of 15 nm in dimension were reported and Al contents of them were investigated using the EDS mapping

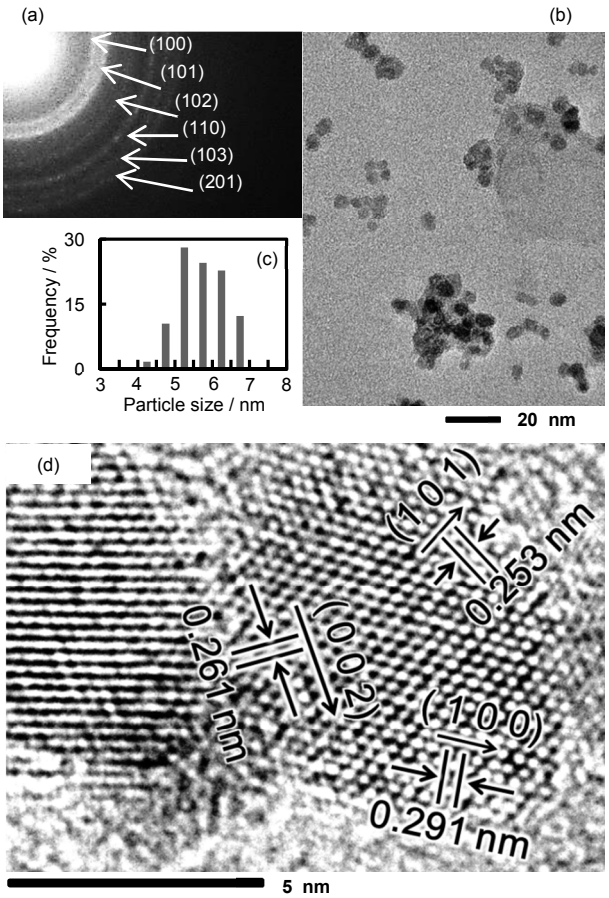

Fig. 1 SAED pattern (a), lower-magnified TEM image (b), size distribution (c), and higher-magnified TEM image (d) of 2% AZO nanoparticles.

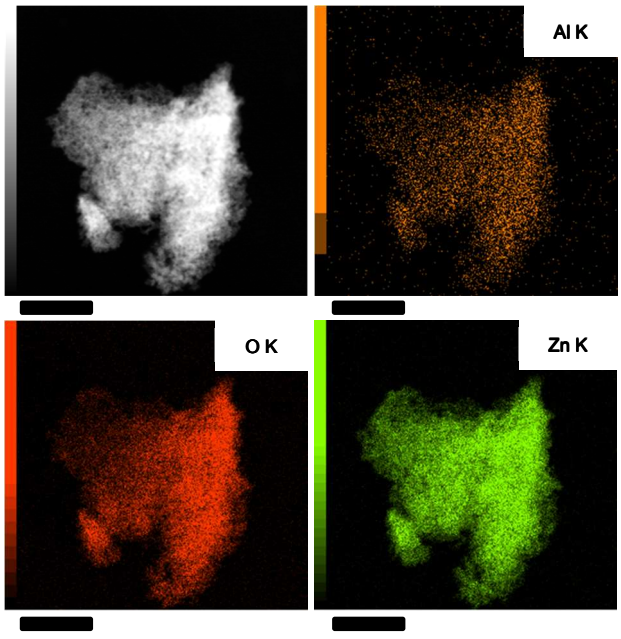

Fig. 2 STEM-HAADF and EDS mapping images of the isolated 2% AZO nanoparticles. Scale bars are 300 nm.

CrystEngComm Accepted Manuscript

tecnique.[30] Similarly, Fig. 2 shows a STEM-HAADF and EDS mapping images of three composition elements of Zn, Al, and O. The Al elements are uniformly distributed, along with the Zn and O elements, throughout an area containing many of the nanoparticles in perspective. The doping molar ratio of Al of the isolated particles was estimated to be 1.9 mol% based on the Zn from the XRF analysis. These results indicate that the isolated white product consists of single-crystalline AZO nanoparticles.

In an FT-IR spectrum of the AZO nanoparticles (Fig. S1), two specific bands at 2967 and 2873 cm^{-1} are assigned to the stretching vibration of the alkyl group, and a shoulder band at 1568 cm^{-1} would be ascribable to the deformation vibration of the amino group. The FT-IR spectrum implies that the AZO nanoparticles adsorb isopropylamines as surface-protecting molecules. The TG profile of the AZO nanoparticles is shown in Fig. S2. Gradual weight loss was observed between 40 and 700ºC and reached 7.49%. In the isolation processes, AZO nanoparticles were obtained at an yield of 0.446 g (99.8% based on the TG weight loss). According to electron ionisation mass spectroscopy synchronised with the TG analysis, the weight loss within the temperature range between 100 and 500ºC mainly corresponded to the water and isopropylamine molecules released from the AZO nanoparticles (Fig. S3).

3.2 Preparation and characterisation of AZO sintering films using precursor dispersion solutions

AZO films with high transparency were successfully fabricated by three-step heating. In the three-step heating program and the corresponding TG profile of the precursor dispersion solution of 2% AZO nanoparticles (Fig. S4), alcohols of the solvent and the excess amounts of isopropylamine were evaporated along with the abrupt weight loss in the first heating step, up to 150ºC. Residue of $(C_3H_7NH_3)NO_3$ was allowed to be melted as a medium for the AZO nanoparticles within a constant temperature of 150ºC, and the $(C_3H_7NH_3)NO_3$ was removed in the second heating step, up to 240ºC based on the weight loss, *vide infra*. In the third heating step, up to 450ºC, the residual AZO nanoparticles were sintered into each other without changing the TG weight. Actually, the white cloudy precursor dispersion solution of 2% AZO nanoparticles spread on a glass substrate was changed *via* the three-step heating processes, as shown in Fig. 3. The white cloudy dispersion solution was changed into a transparent viscous liquid in the first heating step, up to 150ºC (Fig. 3a and b). In the second heating step, up to 240ºC, the viscous liquid was changed into a solid form, and the transparency was maintained through the different states (Fig. 3c). A transparent AZO sintering film of the nanoparticles was successfully obtained in the third heating step, up to 450ºC (Fig. 3d).

A white crystalline powder of isopropylammonium nitrate, $(C_3H_7NH_3)NO_3$, was obtained by a reaction between isopropylamine and nitric acid in methanol.[34] According to the thermogravimetric and differential thermal analysis (TG-DTA) profile and state changes (Fig. S5),[35] the white powdery $(C_3H_7NH_3)NO_3$ was melted above 70ºC with an endothermic

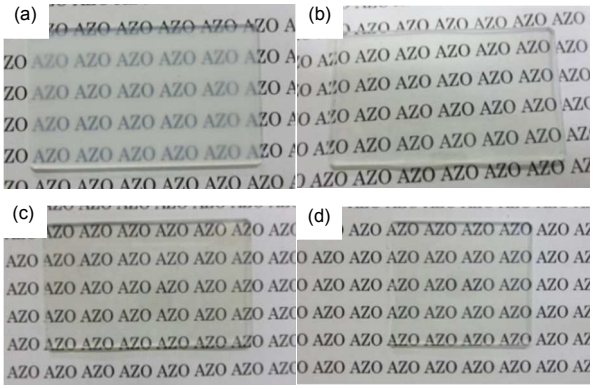

Fig. 3 Photographs of the AZO films before heating (a), after heating at 150ºC (b), 240ºC (c), and 450ºC (d).

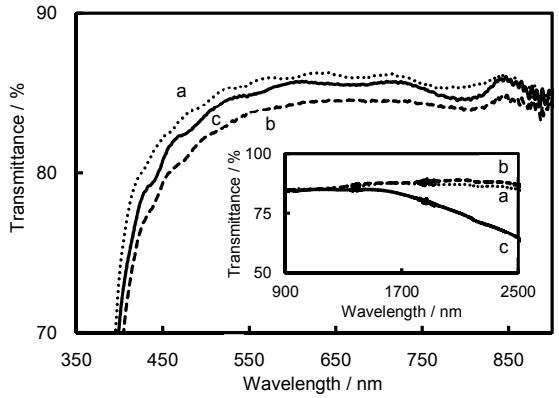

Fig. 4 Transmittance spectra of AZO films heated at 240ºC (a) and 450ºC (b), and after post-annealing in a stream of a mixed gas of N_2 and H_2 (N_2/H_2 = 96 : 4 v/v) at 450ºC (c).

DTA curve and was evaporated above 200ºC with the exothermic TG weight loss. The TG-DTA result supports the validity of the three-step heating process, in which the transparent viscous liquid on the glass substrate at 150ºC is caused by melted $(C_3H_7NH_3)NO_3$, and their evaporation causes a transparent solid to form at 240ºC.

In a typical case, the 2% AZO solid forms on glass substrates heated at 240 and 450ºC show good transparency, and their transmittance reaches more than 80% in the visible region between 400 and 850 nm (Fig. 4). In the XRD patterns, the crystal growth and anisotropic nature of the AZO nanoparticles on a glass substrate were compared between the 2% AZO solid forms heated at 240 and 450ºC along with the isolated AZO nanoparticle powder from the precursor dispersion solution (Fig. 5). The diffraction patterns are consistent with the 2θ peak positions of the hexagonal crystals of ZnO.[32] The mean single-crystal size calculated from the signal widths at half height using Scherrer's equation was 31 nm in the solid film at 240ºC; this was comparable to the 34 nm of the solid film at 450ºC and was much larger than the 6.6 nm of the isolated AZO nanoparticles, implying that the AZO particles effectively grew as single crystals in such a low-temperature medium of $(C_3H_7NH_3)NO_3$ from 150 to 240ºC. In

CrystEngComm Accepted Manuscript

This journal is © The Royal Society of Chemistry 2012

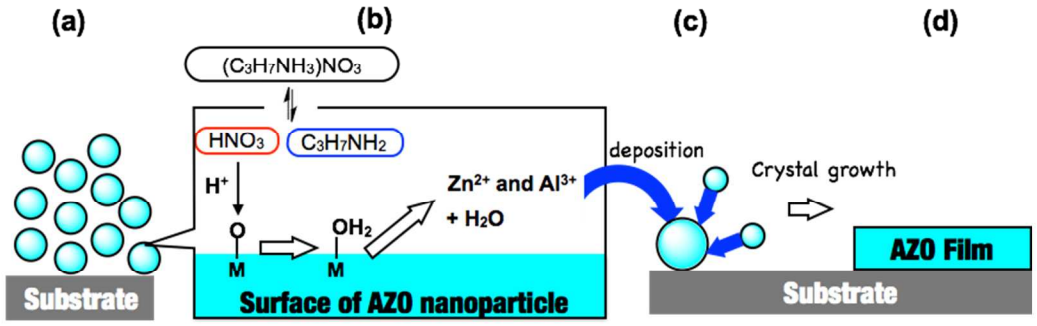

Scheme. 1 Plausible crystal growth mechanism of AZO nanoparticles based on Ostwald ripening.

addition, the anisotropic nature had already appeared in the AZO solid films at 240 and 450ºC on the basis of the intensified XRD signal due to the (002) plane, indicating that the AZO crystals were preferably oriented along the *c*-axis on glass substrates.[36-44]

In equation (1) and (2), the excess amounts of isopropylamine were employed to generate the AZO nanoparticles in the almost quantitative yield (99.8%). In the first heating step at 150ºC, the alcoholic solvent was evaporated along with the excess isopropylamines. In a plausible crystal-growth mechanism of the AZO nanoparticles in the low-temperature medium of $(C_3H_7NH_3)NO_3$ at 150ºC, the AZO nanoparticles would be dispersed in a melted $(C_3H_7NH_3)NO_3$ medium to produce the transparent viscous liquid state (Fig. 3b) without their aggregation (Scheme 1a). This is probably caused by dynamic surface activation as flowing equations:

$$(C_3H_7NH_3)NO_3 \leftrightharpoons C_3H_7NH_2 + HNO_3 \qquad (3)$$

Surface etching (in the case of Zn^{2+} dissolution);

$$ZnO + 2HNO_3 \rightarrow Zn^{2+} + H_2O + 2NO_3^- \qquad (4)$$

Surface deposition by hydrolysis;

$$Zn^{2+} + H_2O + 2C_3H_7NH_2 \rightarrow ZnO + 2C_3H_7NH_3^+ \qquad (5)$$

The metal oxide moieties, Zn-O and Al-O, are exposed on the AZO nanoparticle surfaces. The surface basicity results in surface etching with nitric acid liberated from $(C_3H_7NH_3)NO_3$ (eq. (3) and (4), and Scheme 1 b), and Zn^{2+} and Al^{3+} ions are dissolved into the melted medium of $(C_3H_7NH_3)NO_3$. Liberated $C_3H_7NH_2$ (eq. (3)) may also assist the dissolution of Zn^{2+} and Al^{3+} *via* its coordination bonding ability. The dissolved Zn^{2+} and Al^{3+} can be re-deposited on surfaces of the AZO particles by the hydrolysis reaction (eq. (5)), that is the essentially same reaction as eq. (1). According to Ostwald ripening, the surface etching is usually accelerated in smaller AZO nanoparticles and the surface deposition readily occurs on larger AZO nanoparticles (Scheme 1c). As the result, the AZO nanoparticles apparently grow in crystal size and morphology by such repeated surface etching and deposition processes, and adhered to the glass substrate as an AZO film (Scheme 1d).

In fact, the crystal growth and morphology change of the AZO nanoparticles were investigated in the melted $(C_3H_7NH_3)NO_3$ on a glass substrate at 150ºC. In the heating period at 150ºC up to 12 hours, the AZO nanoparticles

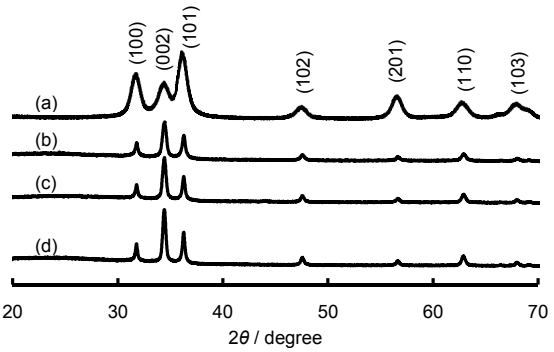

Fig. 5 XRD patterns of the isolated 2% AZO nanoparticles (a), AZO films heated at 240ºC (b) and 450ºC (c), and after post-annealing in a stream of a mixed gas of N_2 and H_2 (N_2/H_2 = 96 : 4 v/v) at 450ºC (d).

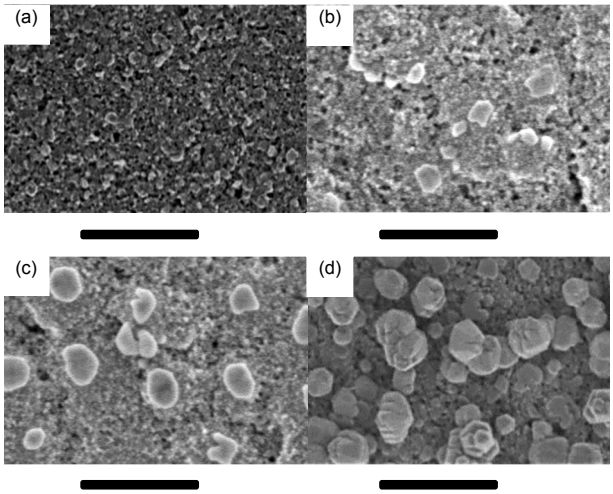

Fig. 6 SEM images of adsorbed AZO crystals on the glass substrate after heating of the precursor dispersion solution at 150ºC for 1 (a), 3 (b), 6 (c) and 12 hours (d). Scale bars are 500 nm.

gradually grew (Fig. 6a to d), and many large hexagonal plates of AZO appeared with much smaller nanoparticles from an FE-SEM image (Fig. 6d). The hexagonal AZO plates notably grew to a sub-micrometre of ~100 nm in size, as compared to other

CrystEngComm Accepted Manuscript

smaller nanoparticles, and were preferably oriented along the *c*-axis on the glass substrate.

The 2% AZO solids adhered to the glass as transparent films after being heated at 240 and 450ºC. In the top-view and cross-section FE-SEM images of the AZO film after the removal of the $(C_3H_7NH_3)NO_3$ at 240ºC, flake particles were observed and grew up to ~100 nm in dimension; nevertheless, much smaller particles of ~10 nm or less were distributed throughout the film (Fig. 7a and b). According to the FE-SEM images of the AZO film at 450ºC, the post-heating prompted fusing among the particles (Fig. 7c and d). In the widely distributed sizes of FE-SEM particles, the mean single-crystal sizes based on the XRD line broadenings were almost unchanged between the AZO films heated at 240 and 450ºC, *vide supra* (Fig. 5). Here, the heating process of the solid film at 450ºC contributes in a limited way to the single-crystal size growth, while it played an important role in improving conductivity of the AZO film by fusing among the particulate interfaces. The resistivity of the 2% AZO sintering film after the heating at 450ºC was 3.4 × 10 Ω cm, estimated from its sheet resistance of 3.4×10^5 Ω/cm^2 as thickness of 1 μm from the SEM image, while the sheet resistance of the film after the heating at 240ºC was out of the range of our resistivity metre. In general, wet-coating using dense dispersion solutions of nanoparticles and sintering of them at higher temperatures are a merit to prepare their thicker films on various substrates; however, such processes have resulted in poor electrical contact *i.e.,* poor charge percolation, among the nanoparticles owing to highly porous morphologies of their films.[32] A similar porous structure has been observed in SEM images of the 2% AZO sintering films even at 450ºC (Fig. 7c and d), and is responsible for the higher resistivity (3.4 × 10 Ω cm) of the film.

3.3 Thickness control of AZO sintering films

In order to control the thickness of the AZO films, we adopted various volumes of the precursor dispersion solution of AZO nanoparticles from 100 to 1000 μL and dropped them on glass substrates. The dropped glass substrates were treated with the three-step heating process, and the cross-section SEM images of the AZO sintering films at 450ºC are shown in Fig. S6. The thickness of the AZO films was almost linearly controllable within the range between 250 nm and 4 μm, depending on the volumes of the precursor dispersion solution (Fig. 8). The viscous liquid of the melted $(C_3H_7NH_3)NO_3$ concentrated AZO nanoparticles was homogeneously spread on the glass and was slowly evaporated. In general, repeated dip- or spin-coating and sintering processes to obtain similar thick films of more than a micrometre consume much time and energy.[38,42,43] This method would be a promising candidate for conveniently controlling the film thickness in a wide range from nanometres to micrometres on the various substrates.

3.4 Improving the electrical conductivity of AZO sintering films by post-annealing with H_2

To improve the electrical conductivity of the film with a thickness of 1 μm, as a typical case, it was post-annealed at 450ºC for 90 min in a stream of a mixed gas of N_2 and H_2. The resistivity of the post-annealed film was drastically improved and reached 4.3×10^{-2} from 3.4 × 10 Ω cm. The electron

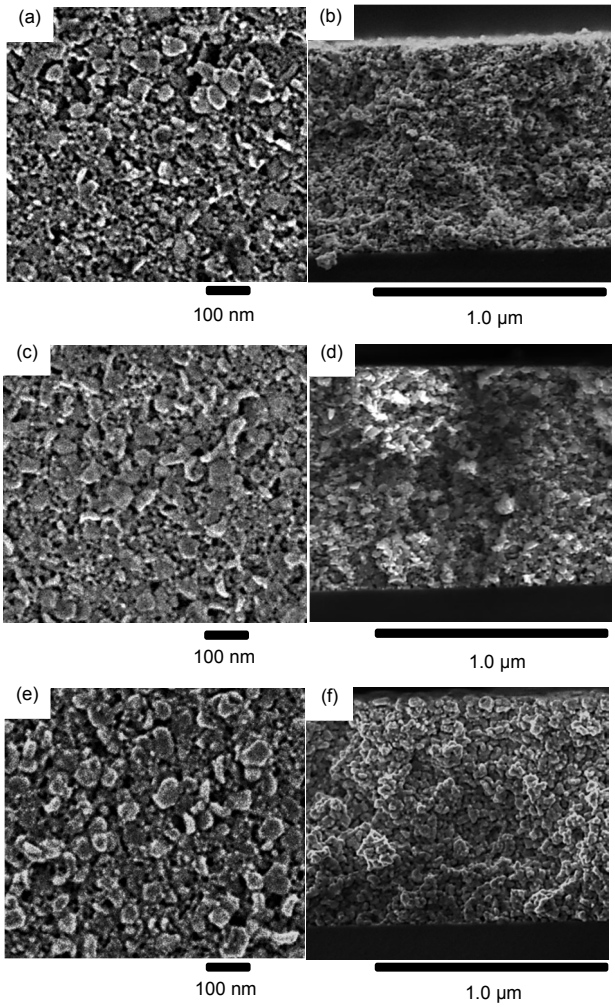

Fig. 7 Top view ((a), (c), and (e)) and cross-section ((b), (d), and (f)) SEM images of the AZO films heated at 240°C ((a) and (b)) and 450°C ((c) and (d)), and after post-annealing in a stream of a mixed gas of N_2 and H_2 (N_2/H_2 = 96 : 4 v/v) at 450ºC ((e) and (f)).

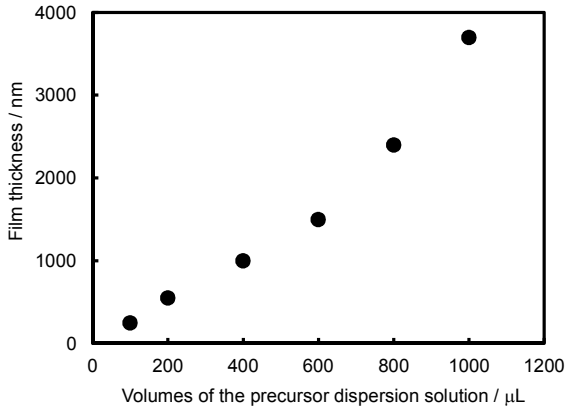

Fig. 8 Plots of thicknesses of the AZO films versus volumes of the precursor dispersion solution used for film preparation.

CrystEngComm Accepted Manuscript

This journal is © The Royal Society of Chemistry 2012

density, volume resistance, and mobility of the 450ºC heated film and the H_2 post-annealed AZO film were investigated (Fig. S7 and Table S1). Both of the films behaved as n-type semiconductors. In the former film, the electron density and carrier mobility were 2.30×10^{18} cm^{-3} and 7.88×10^{-2} cm^2 V^{-1} s^{-1}, respectively. The latter film bore the electron density of 2.97×10^{19} cm^{-3} and the carrier mobility of 4.85 cm^2 V^{-1} s^{-1}. The increase in the electron density of the latter is probably caused by electrons liberated from O^{2-} as oxygen-deficient sites *via* the reaction with H_2.[39-41,44] After the H_2 post-annealing, it was seen that the AZO particles were further fused into each other in the cross-section FE-SEM image of the latter film (Fig. 7e and f), as compared to that of the former. The AZO nanoparticles may be activated on their surfaces by contact with hydrogen molecules, and the surface activation will accelerate their fusing while increasing the number of oxygen-deficient sites. As a result, mobility was also significantly improved to 4.85 from 7.88×10^{-2} cm^2 V^{-1} s^{-1} by developing the electron carrier pathways due to the particulate fusing, *i.e.,* improved electrical contact among the particles. After the H_2 post-annealing, the transparent nature was maintained in the visible region, whereas transmittance in the near-IR regions was decreased (Fig. 4c), implying that the IR reflective ability of the AZO film was enhanced by the increased electron carrier density.[37]

To optimise the Al-doping level, sheet resistances of the AZO films with a thickness of 1 μm after the H_2 post-annealing were measured by changing the molar ratio of Al/Zn between 1.0 and 5.0% (Fig. S8). The sheet resistances were within a range of 10^2 to 10^4 Ω / cm^2. The sheet resistance tends to be improved by increasing the molar ratio of Al/Zn to 2.0% and tends to decrease when increased beyond 2.0%.[38] Therefore, the Al/Zn molar ratio of 2.0% was adopted as the typical case in all of the experiments

4 Conclusions

Alcoholic dispersion solutions of AZO nanoparticles were prepared *via* hydrolysis reactions of $Zn(NO_3)_2$ and $Al(NO_3)_3$ using their own crystal water molecules by adding an excess amount of isopropylamine. The hydrolysis reaction generated a by-product of $(C_3H_7NH_3)NO_3$ in the alcoholic dispersion solutions of AZO nanoparticles. After drop-coating the alcoholic dispersion solution and removing the alcohol solvents at 150ºC, the melted $(C_3H_7NH_3)NO_3$ plays an important role in the viscous liquid dispersion medium for AZO nanoparticles. The AZO nanoparticles can grow up to sub-micrometre dimensions in the melted $(C_3H_7NH_3)NO_3$ through Ostwald ripening. Previously, Teshima *et al*. reported pioneering fabrication methods of various metal oxide films proceeding at relatively high temperatures in the inorganic flux of ionic salts.[12,13] In this study, we unexpectedly discovered $(C_3H_7NH_3)NO_3$ as a low-temperature flux for the crystal growth of AZO nanoparticles. In order to fabricate metal oxide films on the glass substrate, $(C_3H_7NH_3)NO_3$ can be evaporated *via* the liquid form at a much lower temperature, as compared to the usual flux of ionic salts. With an eye towards future reports, we are planning on investigating alkylammonium cations bearing various *normal*, *secondary* and *tertiary* alkyl groups to elucidate the crystal growth mechanism based on the essential roles of the corresponding alkylamines as not only proton-acceptors (eq. (5)) but as coordination ligands assisting dissolution of Zn^{2+} and Al^{3+} ions into their low-temperature fluxes. Such various types of alkylammonium nitrates are our next target as organic-based flux salts suitable for low-temperature crystal growth of various kinds of metal oxide nanoparticles.

Notes and references

[a] Department of Material and Biological Chemistry, Faculty of Science, Yamagata University, 1-4-12 Kojirakawa-machi, Yamagata 990-8560, Japan. Phone and Fax: +81-23-628-4606 Email: kurihara@sci.kj.yamagata-u.ac.jp

[b] National Institute for Material Science, 1-2-1 Sengen, Tsukuba, Ibaraki 305-0047, Japan

† Electronic Supplementary Information (ESI) available: FT-IR spectrum, TG profile, and Mass spectra of AZO nanoparticles, TG profiles of precursor solution including AZO nanoparticles, TG-DTA profile of isopropylammonium nitrate, effects of film thicknesses, Hall resistivity of AZO films and Al doping ratio on sheet resistance. See DOI: 10.1039/b000000x/

1 A. Kolmakov and M. Moskovits, *Annu. Rev. Mater. Res.*, 2004, **34**, 151-180.
2 F. E. Osterloh, *Chem. Soc. Rev.*, 2013, **42**, 2294-2320.
3 P. Poizot, S. Laruelle, S. Grugeon, L. Dupont and J.-M. Tarascon, *Nature*, 2000, **407**, 496-499.
4 L. Castañeda, *Mater. Sci. Appl.*, 2011**,** **2**, 1233-1242.
5 Y. Kobayashi, O. J. Hernandez, T. Sakaguchi, T. Yajima, T. Roisnel, Y. Tsujimoto, M. Morita, Y. Noda, Y. Mogami, A. Kitada, M. Ohkura, S. Hosokawa, Z. Li, K. Hayashi, Y. Kusano, J. Kim, N. Tsuji, A. Fujiwara, Y. Matsushita, K. Yoshimura, K. Takegoshi, M. Inoue, M. Takano and H. Kageyama, *Nat. Mater.*, 2012, **11**, 507–511.
6 X. Fang, J. Yan, L. Hu, H. Liu and P. S. Lee, *Adv. Funct. Mater.*, 2012, **22**, 1613-1622.
7 X. Fang, L. Hu, K. Huo, B. Gao, L. Zhao, M. Liao, P. K. Chu, Y. Bando and D. Golberg, *Adv. Funct. Mater.*, 2011, **21**, 3907-3915.
8 H. Ohta and H. Hosono, *Mater. Today*, 2004, **7**, 42-51.
9 S. Ohkoshi, Y. Tsunobuchi, T. Matsuda, K. Hashimoto, A. Namai, F. Hakoe and H. Tokoro, *Nat. Chem.*, 2010, **2**, 539-545.
10 J. Huan, L. Hu and X. Fang, *ACS Appl. Mater. Interfaces.,* 2014*,* **6**, 1462-1469.
11 N. R. Jana, Y. Chen and X. Peng, *Chem. Mater.*, 2004, **16**, 3931-3935.
12 H. Wagata, T. Wakabayashi. S. Suzuki, M. Tanaka, H. Nishikiori, S. Oishi and K. Teshima, *Cryst. Growth Des.*, 2013, **13**, 1187-1192.
13 Y. Mizuno, N. Zettsu, K. Yubuta, T. Sakaguchi, T. Saito, H. Wagata, S. Oishi and K. Teshima, *Cryst. Growth Des.*, 2014, **14**, 1882−1887.
14 I. Safi, *Surf. Coat. Technol.*, 2000, **127**, 203-219.
15 R. Snyders, J.-P. Dauchot and M. Hecq, *Plasma Processes Polym.*, 2007, **4**, 113–126.

CrystEngComm Accepted Manuscript

16 M. A. E. Khakani, R. Dolbec, A. M. Serventi, M. C. Horrillo, M. Trudeau, R. G. Saint-Jacques, D. G. Rickerby and I. Sayago, *Sens. Actuators B*, 2001, **77**, 383–388.
17 M. G. Tsoutsouva, C. N. Panagopoulos, D. Papadimitriou, I. Fasaki and M. Kompitsas, *Mater. Sci. Eng. B*, 2011, **176**, 480–483.
18 K. L. Choy, *Prog. Mater. Sci.*, 2003, **48**, 57–170.
19 K. Fukuda, T. Sekine, Y. Kobayashi, D. Kumaki, M. Itoh, M. Nagaoka, T. Toda, S. Saito, M. Kurihara, M. Sakamoto and S. Tokito, *Org. Electron.*, 2012, **13**, 1660–1664.
20 K. Fukuda, T. Sekine, Y. Kobayashi, Y. Takeda, M. Shimizu, N. Yamashita, D. Kumaki, M. Itoh, M. Nagaoka, T. Toda, S. Saito, M. Kurihara, M. Sakamoto and S. Tokito, *Org. Electron.*, 2012, **13**, 3296–3301.
21 M. Graf, A. Gurlo, N. Bârsan, U. Weimar and A. Hierlemann, *J. Nanopart. Res.*, 2006, **8**, 823-839.
22 R. N. Gayen, K. Sarkar, S.Hussain, R. Bhar and A. K. Pal, *Indian J. Pure Appl. Phys.*, 2011, **49**, 470-477.
23 C. Goebbert, R. Nonninger, M. A. Aegerter and H. Schmidt, *Thin Solid Films*, 1999, **351**, 79-84.
24 J.-P. Jolivet, S. Cassaignon, C. Chanéac, D. Chiche, O. Durupthy and D. Portehault, *C. R. Chimie*, 2010, **13**, 40-51.
25 L. Wang and M. Muhammed, *J. Mater. Chem.*, 1999, **9**, 2871-2878.
26 M. Yoshimura, W. Suchanek and K.-S. Han, *J. Mater. Chem.*, 1999, **9**, 77-82.
27 K. L. Meagley and S. P. Garcia, *Cryst. Growth Des.*, 2012, **12**, 707-713.
28 S. W. Bian, I. A. Mudunkotuwa, T. Rupasinghe and V. H. Grassian, *Langmuir*, 2011, **27**, 6059–6068.
29 Y. S. Avadhut, J. Weber, E. Hammerberg, C. Feldmann and J. S. Günne, *Phys. Chem. Chem. Phys.*, 2012, **14**, 11610-11625.
30 R. Buonsanti, A. Llordes, S. Aloni, B. A. Helms and D. J. Milliron, *Nano Lett.*, 2011, **11**, 4706-4710.
31 C. S. Prajapati and P. P. Sahay, *Cryst. Res. Technol.*, 2011, **46,** 1086-1092.
32 K. Tarasov and O. Raccurt, *J. Nanopart. Res.*, 2011, **13**, 6717–6724.
33 Z. Lu, J. Zhou, A. wang, N. Wang and X. Yang, *J. Mater. Chem.*, 2011, **21**, 4161-4167.
34 H. Schmid, N. Eisenreich, C. Krause and A. Pfeil, *J. Thermal Anal.*, 1989, **35**, 569-576.
35 The TG-DTA profile was measured using a Shimadzu DTG-60 under a stream of air.
36 N. Rashidi, V. L. Kuznetsov, J. R. Dilworth, M. Pepper, P. J. Dobson and P. P. Edwards, *J. Mater. Chem. C*, 2013, **1**, 6960-6969.
37 Y. Okuhara, T. Kato, H. Matsubara, N. Isu and M. Takata, *Thin Solid Films*, 2011, **519**, 2280–2286.
38 S. P. Shrestha, R. Ghimire, J. J. Nakarmi, Y.-S. Kim, S. Shrestha, C.-Y. Park and J.-H. Boo, *Bull. Korean Chem. Soc.*, 2010, **31**, 112-115.
39 H. Tong, Z. Deng, Z. Liu, C. Huang, J. Huang, H. Lan, C. Wang and Y. Cao, *Appl. Surf. Sci.*, 2011, **257**, 4906-4911.
40 W. Yang, Z. Wu, Z. Liu, A. Pang, Y.-L. Tu and Z. C. Feng, *Thin Solid Films*, 2010, **519**, 31–36.
41 H. Chen, H.-J. Jin, C.-B. Park and G. C. Hoang, *Trans. Electr. Electron. Mater.*, 2009, **10**, 93-96.
42 S. Mondal, K. P. Kanta and P. Mitra, *J. Phys. Sci.*, 2008, **12**, 221-229.
43 H. Zhou, D. Yi, Z. Yu, L. Xiao and J. Li, *Thin Solid Films*, 2007, **515**, 6909-6914.
44 B.-Y. Oh, M.-C. Jeong, D.-S. Kim, W. Lee and J.-M. Myoung, *J. Crystal Growth*, 2005, **281**, 475-480.

CrystEngComm Accepted Manuscript

This journal is © The Royal Society of Chemistry 2012

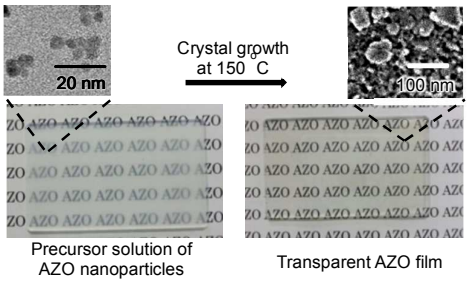

Highly transparent AZO films have been successfully fabricated *via* crystal growth of AZO nanoparticles in a melted isopropylammonium nitrate medium.

CrystEngComm Accepted Manuscript